NEOPLASIA
www.neoplasia.com

Volume 11 Number 3 March 2009 pp. 220–227 220

In Vivo Investigation of Breast Cancer Progression by Use of an Internal Control[1]

John Baeten[*,†,‡,2], Jodi Haller[‡,2], Helen Shih[‡] and Vasilis Ntziachristos[*,†,‡]

*Institute for Biological and Medical Imaging (IBMI), Helmholtz Zentrum München, Neuherberg, Germany; [†]School of Medicine and School for Electrical Engineering and Information Technology, Technische Universität München, München, Germany; [‡]Laboratory for Bio-optics and Molecular Imaging, Center for Molecular Imaging Research, Massachusetts General Hospital, Harvard Medical School, Charlestown, Boston, MA 02129, USA

Abstract

Optical imaging of breast cancer has been considered for detecting functional and molecular characteristics of diseases in clinical and preclinical settings. Applied to laboratory research, photonic investigations offer a highly versatile tool for preclinical imaging and drug discovery. A particular advantage of the optical method is the availability of multiple spectral bands for performing imaging. Herein, we capitalize on this feature to demonstrate how it is possible to use different wavelengths to offer internal controls and significantly improve the observation accuracy in molecular imaging applications. In particular, we show the independent *in vivo* detection of cysteine proteases along with tumor permeability and interstitial volume measurements using a dual-wavelength approach. To generate results with a view toward clinically geared studies, a transgenic Her2/*neu* mouse model that spontaneously developed mammary tumors was used. *In vivo* findings were validated against conventional *ex vivo* tests such as histology and Western blot analyses. By correcting for biodistribution parameters, the dual-wavelength method increases the accuracy of molecular observations by separating true molecular target from probe biodistribution. As such, the method is highly appropriate for molecular imaging studies where often probe delivery and target presence are not independently assessed. On the basis of these findings, we propose the dual-wavelength/normalization approach as an essential method for drug discovery and preclinical imaging studies.

Neoplasia (2009) 11, 220–227

Introduction

With an increasing shift toward studying functional interactions at the cellular and subcellular levels, postgenome biology can significantly benefit from observation tools with the ability to offer quantitative functional and molecular parameters at different system levels. Noninvasive fluorescence imaging has recently emerged as a visualization tool with a high versatility in studying disease and therapeutic efficacy biomarkers. Largely enabled by the emergence of several new adept fluorescence proteins and probes with high *in vivo* labeling capacity, fluorescence observation has the potential to become a mainstream biomedical investigation tool. A particular strength lies with the use of advanced imaging methods, which, in contrast to simple planar (photographic) imaging, can offer true quantification and accuracy. Advanced imaging methods have now been applied toward imaging cellular receptors [1–3], proteases [4–7], and chemotherapeutic effects [8–10].

However, compared with other imaging modalities, fluorescence molecular imaging is still confronted by the inability to independently assess the amount of target present over the delivery of the molecular

Abbreviations: MMP, matrix metalloproteinase; NFRI, near infrared fluorescence reflectance imaging; ROI, region of interest

Address all correspondence to: Vasilis Ntziachristos, Institute for Biological and Medical Imaging, Helmholtz Zentrum München, Ingolstädter Landstraße 1, D-85764 Neuherberg, Germany, or Technische Univeristät München, Klinikum Rechts Der Isar, Trogerstr. 32, 81675 München, Germany. E-mail: v.ntziachristos@tum.de

[1]The work in this investigation was supported by the US Army Medical Research and Materiel Command Award W81XW-04-1-0239 and National Institutes of Health (NIBIB) grant no. RO1EB004382.

[2]These authors equally contributed to this work.

Received 30 May 2008; Revised 3 December 2008; Accepted 8 December 2008

DOI 10.1593/neo.08648

probe used. The particular difficulty is that most of fluorescence molecular imaging is currently static; that is, it is obtained after the probe is delivered and after binding or activation processes have reached steady state. As such, it contains no transients or dynamic features that could be used to obtain delivery and uptake metrics. This is particularly challenging when using molecular probes designed to stay in circulation for long times [11] to maximize tumoral delivery. Thus, any signal collected is a function of the target concentration and of the probe's availability at the target site (efficiency of probe delivery), which can lead to significant quantification inaccuracies if not accounted for. Furthermore, given that different tumor types and treatment regimes (e.g., antiangiogenic treatment) can modulate cancerous tissue permeability, accounting for target presence and biodistribution at the region of interest (ROI) is of great importance.

As such, we consider a dual-wavelength strategy and show how it can be used to improve on the coupled nature of fluorescence imaging signals. Dual-wavelength imaging has been used before to resolve multiple targets. For example, in a study done by Montet et al. [12], two nearly identical vascular probes excitable at separate wavelengths were used to monitor and measure vasculature volumes in mice and observe different angiogenic inhibitor efficacies. Additionally, a study done by Nahrendorf et al. [13] established how dual-channel imaging could be used to investigate the spatiotemporal resolution of both phagocytic and proteolytic activities mediated by macrophages and neutrophils in the same mouse.

Instead, herein, we use one wavelength to image an activatable fluorescent probe and a second wavelength to image a fluorescent probe that reveals nonspecific probe delivery and uptake. By decomposing biodistribution specifics from the signals collected, accurate target presence can then be inferred. We selected to visualize tumor cathepsins and matrix metalloproteinases (MMPs) contents owing to their elevated levels in cancers [14], using fluorescent probes that do not emit fluorescence until they interact with proteases [15]. To showcase the method in a clinically relevant tumor model, we used a transgenic Her2/*neu* mouse model that spontaneously developed focal mammary tumors. Doing so, we demonstrate improved accuracy of the dual-wavelength approach over conventional single-wavelength planar fluorescence imaging and discuss how the dual-wavelength method yields a generic and essential strategy by which physiological and molecular readings can be decomposed to offer true quantitative readings.

Materials and Methods

Imaging System

Imaging was performed in normalized epi-illumination (reflectance) imaging mode. Normalized epi-illumination is a technique developed to overcome limitations of conventional photographic approaches and corrects fluorescence signals by corresponding measurements of light attenuation in tissue [16]. The imaging system shown in Figure 1 allowed for epi-illumination data acquisition and has been fully described before [17]. In short, white light illumination was achieved using a fluorescent bulb placed 30 cm from the animal, whereas narrow band illumination was performed using two 672- and 748-nm CW laser diodes (B&W Tek, Newark, DE) routed to an optical switch (DiCon FiberOptics, Berkley, CA) for multimodal and multispectral imaging. The laser output from the switch was then directed to a beam expander that broadened the beam on the surface of the animal. Photons generated within the animal were

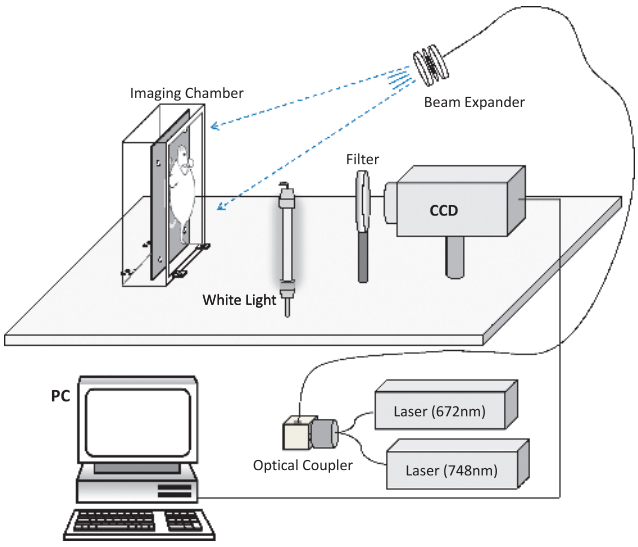

Figure 1. Multispectral multimodal imaging system schematic. Configuration allowed for investigations of epi-illumination imaging at two wavelengths (672 and 748 nm).

then detected by a 512 × 512-pixel array CCD camera (Roper Scientific, Trenton, NJ), outfitted with the appropriate band-pass filters for the wavelengths used. Specifically, two different band-pass filters (Andover, Salem, NH) were tuned at the excitation and emission peaks of the fluorescent probes (AngioSense 670-Cy5.5 channel, excitation: 670 ± 5 nm, emission: 710 ± 10 nm; and ProSense 750-AF750 channel, excitation: 750 ± 5 nm, emission: 800 ± 20 nm). No filter was used for white light images.

Animal Model and Imaging

In this study, FVB/N-Tg (MMTV*neu*) 202 Mul/J, (homozygous for the MMTV*neu* rat transgene) breeder pairs were obtained from Jackson Laboratories (Bar Harbor, ME), and controlled breedings were conducted. Progeny was raised until 4 months of age, at which time focal mammary tumors began to develop exclusively in females (100% development by age 6 months). During this time, tumor development was monitored with weekly palpation and/or caliper measurements preceding each imaging session and continued for a number of weeks (enabling a range of tumor sizes for correlative demonstration of protease activity levels). FVB/NJ mice, the nontransgenic parental strain (Jackson Laboratories), were screened in parallel as controls because they typically do not develop spontaneous tumors in contrast to the spontaneous focal mammary adenocarcinoma development seen among the MMTV*neu* females only. The mouse colony was then divided into two groups so that cathepsins and MMPs could be assessed in separate animals; this also enabled accommodation of the spectral properties of the *in vivo* probes involved. Specifically, this study included 31 MMTV*neu* transgenic female mice (21 cathepsins and 10 MMPs) to investigate protease expression and 3 FVB/NJ as background control animals. The subsets of experimental animals were dictated by the stochastic nature of the tumor model as the development of multiple tumors proceeded quite rapidly after the onset of the primary lesion. Only those animals in which the primary tumor had not exceeded a critical size were able to remain for multiple image sessions necessary for longitudinal study. Furthermore, to provide a sufficient range of tumor specimens per

size classification used ($N \geq 3$; Figure 4), the indicated number of MMTV*neu* mice was included.

All animal studies were performed according to protocol approved by the Institutional Animal Care and Use Committee Review Board and Massachusetts General Hospital Center for Comparative Medicine. Twenty-four hours before each imaging session, while under isoflurane narcosis, mice were shaven and treated with Nair (Church & Dwight Co., Inc., Princeton, NJ) to remove hair. Also, at this time, mice received either one of the intravital cysteine protease probes of interest (cathepsin: ProSense 750; MMP: MMPSense 680) as well as a probe to account for vascularization and biodistribution (AngioSense 680 or 750, respectively; VisEn Medical, Inc., Woburn, MA) by tail vein injection. Per manufacturer's recommendations, the *in vivo* imaging agents were administered per average 25-g mouse in the following dosages: ProSense 750, 0.08 mg/0.025 kg; MMPsense, 0.09 mg/0.025 kg; and AngioSense 750/680, 0.05 mg/0.025 kg. Each probe was given in 2-nmol concentrations.

For imaging, animals were anesthetized with ketamine/xylazin and were positioned in the optical chamber. All animals were softly compressed against a glass window and maintained an approximate thickness of 1.3 cm for ensuring uniform imaging and identical imaging parameters and placement throughout all measurements. Mice were then imaged at the onset of lesion development, tumors ranging from ~1 to 15 mm, with some mice being imaged for several weeks. Once tumors reached the upper limit of the study (i.e., ~15 mm) or when interrogations were completed, animals were euthanized with carbon dioxide asphyxiation and tumors were harvested and snap frozen for *ex vivo* analysis. Smaller tumors were confirmed (i.e., <5 mm) by following their growth over time in longitudinal studies (this growth followed on a per animal basis every 3-5 days by visual inspection or fluorescence imaging) and by histology.

Ex Vivo *Analysis*

Ex vivo analyses were performed to provide correlative biologic confirmation of the protease activity indicated through noninvasive *in vivo* imaging. To do so, various routine *ex vivo* techniques were performed to characterize the presence and relative amounts of cathepsins and MMPs required to activate the probes used. The following section details the steps required and reasons for each analysis.

Immunohistochemistry. Immunohistochemical analyses were performed to demonstrate immunohistochemical evidence of specific cathepsin B and MMP-9 expression in extracted tumor regions. Five-micrometer sections of freshly frozen tumor samples were examined for expression of cathepsin B (Santa Cruz Biotechnology Inc., Santa Cruz, CA) or MMP-9 (Abcam, Inc., Cambridge, MA). Biotinylated secondary antibodies were applied (Vector Laboratories, Burlingame, CA) as the avidin-biotin peroxidase method (standard Vectastain ABC Kit; Vector Laboratories) and the AEC Substrate Chromagen (Dakocytomation, Dako North America, Carpinteria, CA; as per manufacturer's recommendations) were used. The red reaction product was visualized with 3-amino-9-athyl-carbazol substrate (AEC; Dakocytomation). Subsequent haemotoxylin counterstaining was performed for all tissues.

Western blots. Given that none of the primary antibodies used in the immunohistochemical analyses were capable of distinguishing between latent and active forms of the involved proteases, Western analysis of the active form of a specific protease was critical in deriving accurate correlations. As such, densitometric analyses of Western blots were used to confirm corresponding cathepsin B and MMP-9 protein content of the tumor samples. In short, tumors were excised (specifically a core and margin sample was taken from each tumor with a third adjacent sample of mammary adipose collected from within a 1-cm perimeter of each growth, respectively) and homogenized in lysis buffer. After total protein determination (Pierce BCA protein assay; Pierce Biotechnology, Rockford, IL), 5 μg of total protein lysate was subjected to electrophoresis on 12.5% SDS-PAGE followed by its transfer to methanol-equilibrated polyvinylidene fluoride membrane (Bio-Rad Laboratories, Hercules, CA) according to the manufacturer's instructions. Concentrations for blotting anti–cathepsin B, anti–MMP-9, and HRP-labeled secondary antibody followed manufacturer's recommendations (R&D Systems, Minneapolis MN). The blots were developed with the enhanced chemiluminescence system (Amersham Pharmacia Biosciences, Piscataway, NJ). The immunoblot of GAPDH (R&D Systems) was used as a loading control. Also, additional confirmation of heightened enzymatic activity of MMP-9 within tumor samples was provided through densitometric analysis of its characteristic 97-kDa lysis band apparent after gelatin zymography (data not shown).

Data Acquisition and Analysis

To tabulate signal strength acquired from epi-illumination imaging, the fluorescent images were exported to ImageJ (National Institutes of Health, Bethesda, MD). The *Freehand selections* tool in ImageJ was then used to delineate complete adenocarcinomas by following contours that were of fluorescence strength that was at least that of the background fluorescence. These contours where referred to as the ROI (unique shape and number of pixels) for a given tumor. The ROI was then transposed onto the contralateral mammary fat pad to obtain a measure of nondiseased tissue fluorescence. Furthermore, these ROIs were used, namely, their size, shape, and location (determined by x and y coordinates), between the multispectral images (i.e., images acquired at the two wavelengths of interest) to minimize user bias and variances between the same animal. Once the contour areas had been determined, mean signals were obtained from the ROIs using the *Measure* feature found under the *Analyze* dropdown menu.

A similar protocol was used to obtain quantitative information from the Western blots. Specifically, densitometry was performed on the radiographs generated from each of three separate Western analyses (i.e., core, margin, and adjacent tissues) for each tumor using ImageJ software. In particular, the active protease bands on the Western blots for each individual tissue sample were delineated, and mean values were tabulated and added to produce a singular value for active protease. To generate a measure of the total protease expression *ex vivo* at the protein level, the mean signal values from the core, margin, and adjacent tissue Western blots were then combined for each tumor. The rationale for collecting tissue specimens in this manner stems from the reports of macrophages, stromal fibroblasts adjacent to the tumor, as well as carcinoma cells themselves expressing varying degrees of cathepsin B in a variety of solid tumors [18], including breast cancer [19]. Similar data on spatially varying MMP-9 expression have been collected regarding tumoral and stromal cells. In fact, elevation of stromal MMP-9 levels has been associated with more aggressive poorly differentiated lesions [20–22] relative to that of survival advantage inferred with greater MMP-9 expression within the carcinoma cells themselves.

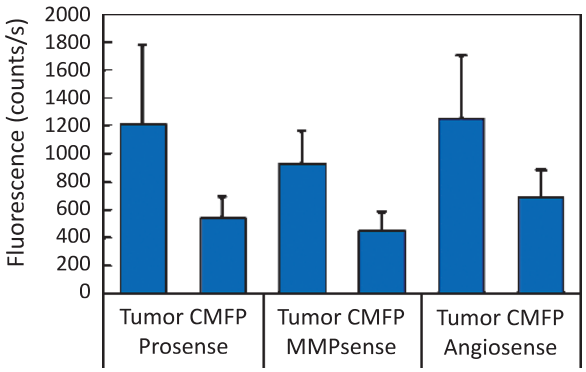

Figure 2. *In vivo* NFRI signals obtained from tumor and nondiseased contralateral mammary fat pad (CMFP) tissue for each probe of interest. All signal values obtained from adenocarcinomas are statistically higher than background; however, ProSense expression is detected at a much higher extent compared with MMPSense. AngioSense is a nonspecific probe used in this study to account for probe delivery.

Data are presented as mean ± SD. Statistical analysis of *in vivo* tumor fluorescence was conducted using a 2-tailed, unpaired Student's *t*-test (where N = 21, 10, and 31 for ProSense, MMPsense, and AngioSense, respectively), or a single-factor analysis of variance (ANOVA; where $N \geq 3$ for each subset). In both cases, a P value of $\leq .05$ was considered to be statistically significant.

Results

In Vivo *Epi-illumination Imaging*

Inspection of raw images acquired by near-infrared fluorescence reflectance imaging (NFRI) revealed that cancerous regions were clearly visible based solely on signal intensities for each probe. Collectively, findings from 31 mice (21 ProSense and 10 MMPSense) are shown in Figure 2. As observed, tumor fluorescence is 2.2, 2.0, and 1.9 times higher than background fluorescence measured in contralateral mammary fat pad tissue for ProSense, MMPSense, and AngioSense, respectively. Further analysis confirms that tumor signals are statistically higher (unpaired Student's *t*-test) than nondiseased mammary fat pad tissue as evident by P values $<.05$. Specifically, P values $>.01$ for ProSense, MMPSense, and AngioSense.

Despite fluorescence signals being elevated in cancerous regions, fluorescence intensities corresponding to protease activities did not deviate considerably between tumor sizes/progressions. This is visually evident in the example provided in Figure 3 and is further substantiated for all cases in Figure 4. In particular, Figure 3 displays dual-wavelength *in vivo* epi-illumination images acquired from two different mice, both mice being 5 months old, that have developed mammary tumors of varying sizes and developmental stages. The *top panel* presents an interrogation of cathepsin protease activity in a mouse with two tumors (L: 13 × 13 mm and M: 8 × 8 mm), and the *bottom panel* presents an interrogation of MMP protease activity in a mouse with three tumors (M: 9 × 6 and 10 × 8 mm and S: 3 × 3 mm). White light images are provided to identify the tumor category and location; where S, M, and L stand for small, medium, and large tumors (Figure 3*A*). Shown in Figure 3*B* are the fluorescent signals obtained from the AngioSense marker, which relate to vascularization and the biodistribution of the protease probes. Here, it is observed that AngioSense does accumulate in the cancerous region and that fluorescence intensities do vary considerably between tumors. However, consulting Figure 3*C*, we see that although fluorescence from protease probes is higher in diseased tissue compared with healthy tissue (outlying mammary fat pad), tumor size/development is undetectable by monitoring cysteine protease

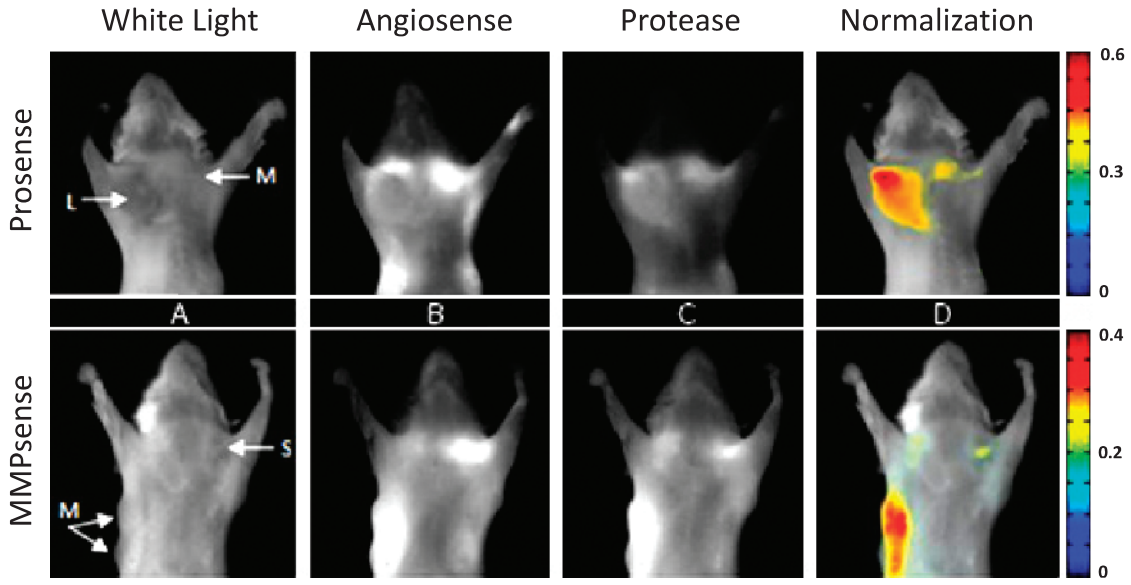

Figure 3. *In vivo* dual-wavelength epi-illumination images of cysteine protease expression in transgenic mammary tumor-forming mice. (A) White light image identifies tumor location and category: S indicates small, M, medium, L, large tumors. (B) AngioSense channel shows an accumulation of probe in tumor and represents vascularization and biodistribution of activatable probe. (C) Protease channel (either ProSense or MMPSense) shows accumulation of probe in tumor, but tumor size is not ascertainable by expression levels. (D) Superposition of protease signal divided by AngioSense signal with white light image shows how dual-wavelength/normalization approach can improve the observation accuracy.

expressions only. Particularly, mean fluorescence values obtained from delineating the entire lesion produces values independent of malignancy growth. These results are most evident in the ProSense epi-illumination image (Figure 3*C*, *top panel*), where protease expression level alone functions as a poor correlate of lesion size. Nevertheless, as observed in Figure 3*D*, when cysteine protease expressions are corrected for by an internal control that accounts for probe delivery, malignancies are discernible by size and developmental stage. In fact, by normalizing protease expressions to their equivalent biodistribution, signal values become two to three times higher between each tumor category (i.e., small, medium, and large).

Figure 4 confirms the findings presented in Figure 3 for the entire data set used to compare *in vivo* measurements with the *ex vivo* tests preformed herein. Specifically, Figure 4 shows results from 12 mice (14 tumors) from the cathepsin protease data set (Figure 4, *A* and *B*) and 6 mice (13 tumors) from the MMP protease data set (Figure 4, *C* and *D*). As observed, raw ProSense and MMPSense expression obtained from cancerous regions remains fairly constant for tumors of various sizes, which is not due to the lack of available protease probe as confirmed by the AngioSense signal (Figure 3, *A* and *C*, respectively). In fact, by grouping growths into categorical areas ($N \geq 3$ for each category) and performing a single-factor ANOVA, we find that overall fluorescent protease expression does not statistically increase for larger tumors (~1 cm or more in length and width) beyond the levels seen for medium- (5-10 mm in length and width) or smaller- (5 mm or less in length and width) diameter tumors for both protease activatable probes (P values of .210 and .126 for ProSense and MMPSense, respectively). Note that tumor size was calculated as a two-dimensional measure using caliper measurements of a long and a short axis. The areas calculated were consistent with the area seen on the white light images at all cases where the tumor was clearly visible.

Nevertheless, given that expression levels remain nearly constant among lesions, the data indicate considerable capacity for successful identification of tumors as small as 2 mm in diameter by investigating molecular signatures. However, taking a similar approach but instead dividing the fluorescent signals of either ProSense or MMPSense to their corresponding biodistribution signals (i.e., AngioSense), we see that a possible correction is available to monitor protease expression as a function of tumor size (Figure 4, *B* and *D*, respectively). Furthermore, as confirmed by P values < .01 (single-factor ANOVA), this method provides a way to monitor disease progression (i.e.,

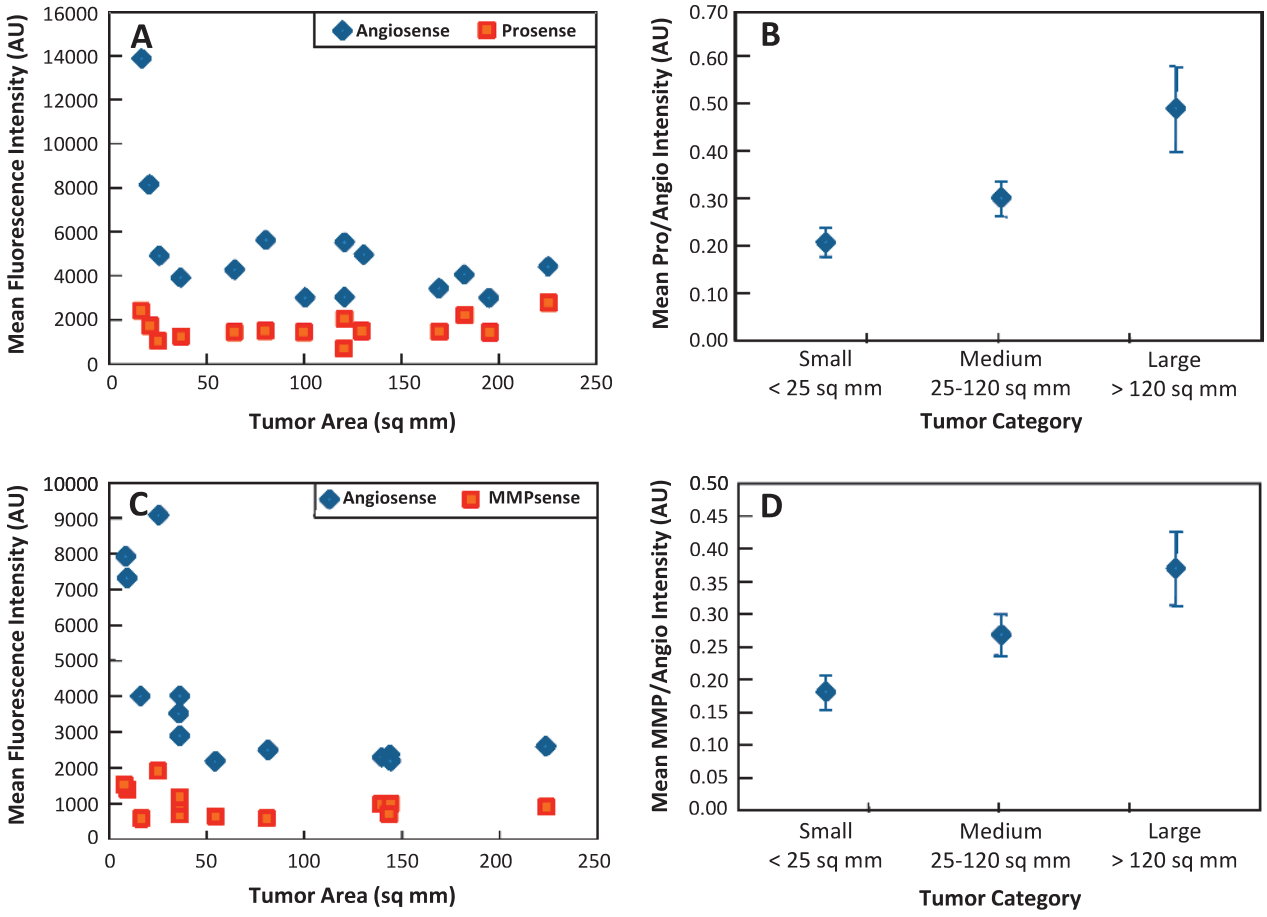

Figure 4. *In vivo* protease signals from tumors of various sizes either plotted with or normalized to corresponding vascular signals. Raw mean ProSense (A) and MMPSense (C) along with AngioSense signals for each tumor. As seen, protease expressions remain rather constant and are statistically independent of tumor size, which is not caused by a lack of available protease probe at the cancerous region as evident by AngioSense signals. Mean ProSense (B) and MMPSense (D) expressions normalized to respective biodistribution signals (AngioSense) for tumors of different categorical areas. This internal control provides a statistically relevant way to observe disease progression.

increasing protease expression over time) *in vivo* from both ProSense and MMPSense signals.

Ex Vivo *Correlative Studies*

Immunohistochemistry showed clear up-regulation of cathepsin-B as well as MMP-9 from harvested tumors, which represent key enzymes for probe activation of ProSense and MMPSense, respectively. As such, signals acquired at tumor sites are undoubtedly from probe activation and, moreover, from proteases known to be overexpressed in aggressive tumors. Correlative *ex vivo* histology confirmed the initial imaging findings in that exposure times are considerably less for investigations with ProSense over MMPSense, suggesting that higher accumulation and expression of the ProSense marker was occurring. Furthermore, as seen in Figure 5, correlative *ex vivo* histology shows a strikingly improved correlation with *in vivo* measurements when protease signals are corrected for probe delivery. More specifically, Figure 5 represents how raw ProSense (Figure 5*A*) and MMPSense (Figure 5*C*) *in vivo* signals show no correlation with the true protein levels, but when ProSense (Figure 5*B*) and MMPSense (Figure 5*D*) signals are corrected by their biodistribution (i.e., division with the AngioSense signals), the *in vivo* signals correlate to the underlying physiology and true protein levels contained in the tumors, as seen by the improved values for the coefficient of determination (R^2).

Discussion

An increasing number of optical imaging studies have shown the ability to visualize cellular and subcellular processes in intact tissues [1–10,23–27] after the development of several technologies to fluorescently tag tissue, disease, and therapeutic efficacy biomarkers *in vivo* [8,9,28–35]. Although the feasibility and value of fluorescence imaging have been amply demonstrated, it has become crucial to develop strategies that accurately report on the underlying cellular and subcellular activities. To improve quantification, approaches that account for the effects of the tissue optical heterogeneity and the fluorescence activity depth on signal intensity have been considered [36]. Such methods typically focus on the use of physical models of photon propagation in tissue to analytically correct for propagation effects. In this study, we addressed a remaining important aspect of imaging accuracy, that is, the separation of probe uptake and target presence, with the ultimate goal of accurately quantifying the actual target presence. The underlying limitation considered is that the light

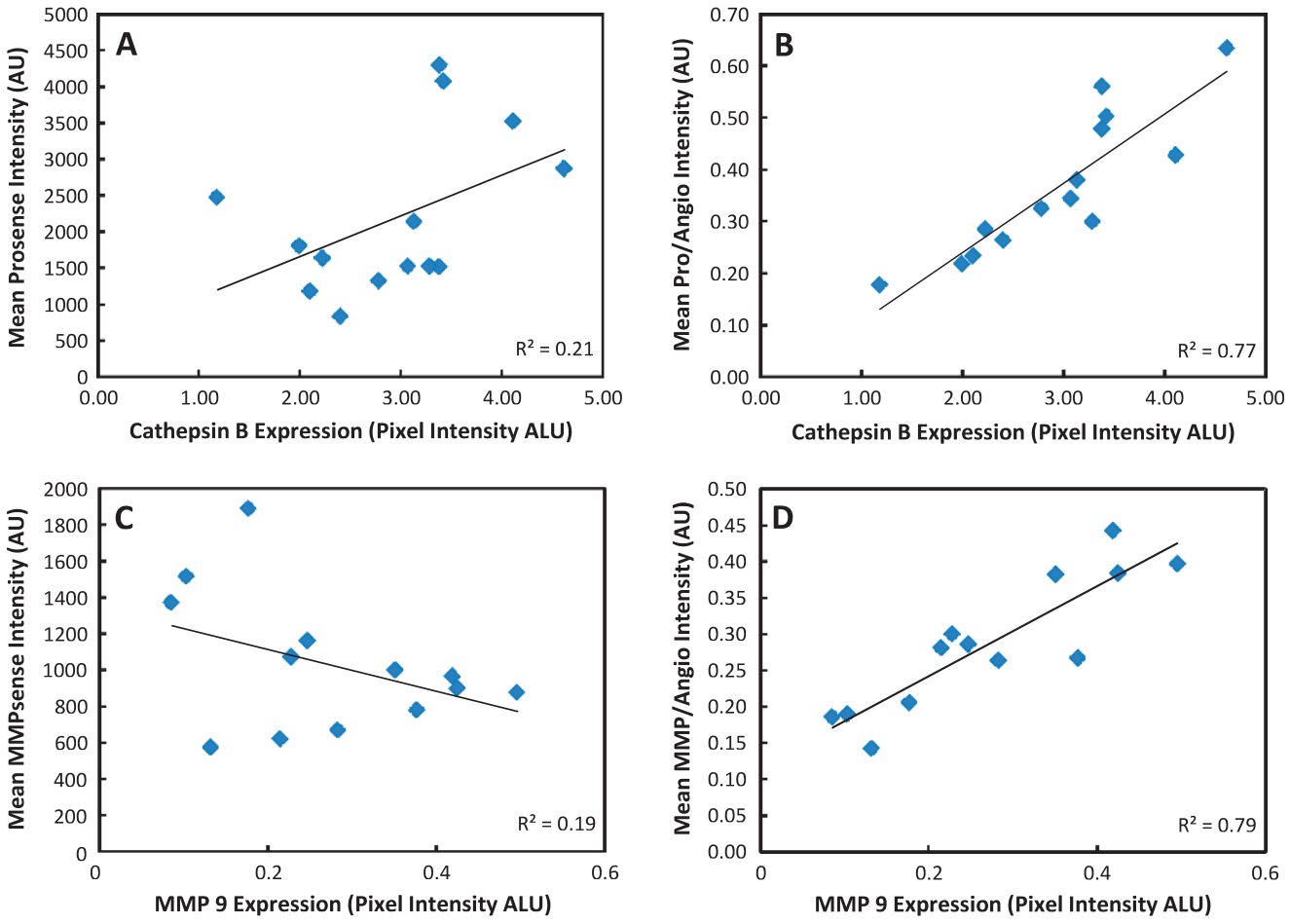

Figure 5. *In vivo* fluorescence signals plotted against *ex vivo* signals obtained by Western blot analyses. Mean ProSense (A) and MMPSense (C) signals plotted against corresponding total protein level expressions. Mean ProSense (B) and MMPSense (D) normalized to drug delivery (i.e., divided by AngioSense) plotted against corresponding total protein level expressions. Normalizing *in vivo* protease signals with biodistribution signals allows for an internal correction that also provides an improved correlation to the underlying physiology.

strength recorded *in vivo* using a fluorescent probe with specificity to a certain target depends on the amount of the target present and the efficiency of the probe uptake. The most obvious shortcoming is that the absence of fluorescence signal, for example, can be any combination of lack of target or lack of delivery/uptake at the time point of observation making the interpretation of the corresponding single-wavelength measurement highly unreliable.

For this reason, we used a dual-probe/dual-wavelength approach to establish an internal control, that is, a background measurement from the same animal where the target measurement was acquired from. This has been showcased herein by using a common protease activatable probe (in one spectral channel) for visualizing a tumor biomarker, together with a probe of similar biodistribution (in a separate spectral channel) which corresponded to probe delivery. In this approach, an identical molecule to the activatable probe (but without the activation mechanism) was used to reveal background and tumor uptake. However, more generally, this technique can also be used with targeted probes (such as antibody-, antibody fragment–, or peptide-based probes) where the targeting capacity (affinity) mechanism of the control probe is scrambled to prevent binding.

We further selected a model of spontaneous breast cancer, which more closely resembles human tumor development compared with mouse models inoculated with cancer cells. *In vivo* measurements demonstrated a variation in probe uptake by different tumors and tumor sizes. Compared with single-wavelength (uncorrected) measurements, dual-wavelength protease measurements corrected for probe uptake exhibited significantly better correlation with the protease content, as recorded by densitometry analysis performed on standardized Western blots. Regarding malignancy detection, we found that tumors as small as 2 to 3 mm in diameter demonstrated a 2:1 contrast over background and that protease expression did not statistically increase for larger tumors (~1 cm or more in length and width) beyond the levels measured from smaller lesions (5 mm or less). These data may also prove relevant for primary tumor detection or as a biomarker in monitoring therapeutic response, for instance, to inhibitor compounds being introduced to clinical trials.

In summary, the data in this article were reported using epifluorescence imaging, which is limited to surface weighting observations, that is, 2- to 3-mm sampling depth. An additional advantage of the dual-wavelength method in epi-illumination measurements is that changes in signal strength due to depth or optical heterogeneity (darker lesions *vs* lighter lesions) do not significantly affect the corrected measurement. However, this correction technique applies so long as the two emission bands are spectrally close to each other and lie in the near infrared—where relatively small attenuation variations are present as a function of wavelength. Regardless, the use of tomographic methods with the dual-wavelength approach could further improve quantification and offer a three-dimensional picture of fluorochrome biodistribution. As such, the use of dual-wavelength imaging for establishing internal controls can 1) offer a more accurate strategy in cases where probe uptake may exhibit variations, 2) offer more accurate biologic observations *in vivo*, and 3) be extended to multiple wavelengths which, typically in pairs, could offer improved observation accuracies of more than one target.

Acknowledgments

The authors thank Elena Aikawa, Yoshiko Iwamoto, and Todd Sponholtz of the Pathology Core CMIR facility for their support.

References

[1] Barrett T, Koyama Y, Hama Y, Ravizzini G, Shin IS, Jang B-S, Paik CH, Choyke PL, and Kobayashi H (2007). Molecular imaging for typing epidermal growth factor receptors expressed on tumor cells using a cocktail of two monoclonal antibodies conjugated with two distinct near infrared fluorophores. *Clin Cancer Res* **15**, 6639–6648.

[2] Koyama Y, Barrett T, Hama Y, Ravizzini G, Choyke PL, and Kobayashi H (2007). *In vivo* molecular imaging to diagnose and subtype tumors through receptor-targeted optically labeled monoclonal antibodies. *Neoplasia* **9**, 1021–1029.

[3] Montet X, Ntziachristos V, Grimm J, and Weissleder R (2005). Tomographic fluorescence mapping of tumor targets. *Cancer Res* **15**, 6330–6336.

[4] Bremer C, Ntziachristos V, Weitkamp B, Theilmeier G, Heindel W, and Weissleder R (2005). Optical imaging of spontaneous breast tumors using protease sensing "smart" optical probes. *Invest Radiol* **40**, 321–327.

[5] Deguchi JO, Aikawa M, Tung CH, Aikawa E, Kim DE, Ntziachristos V, Weissleder R, and Libby P (2006). Inflammation in atherosclerosis: visualizing matrix metalloproteinase action in macrophages *in vivo*. *Circulation* **114**, 55–62.

[6] Wunder A, Tung CH, Müller-Ladner U, Weissleder R, and Mahmood U (2004). *In vivo* imaging of protease activity in arthritis: a novel approach for monitoring treatment response. *Arthritis Rheum* **50**, 2459–2465.

[7] Haller J, Hyde D, Deliolanis N, de Kleine R, Niedre M, and Ntziachristos V (2008). Visualization of pulmonary inflammation using noninvasive fluorescence molecular imaging. *J Appl Physiol* **104**, 795–802.

[8] Ntziachristos V, Schellenberger EA, Ripoll J, Yessayan D, Graves E, Bogdanov A Jr, Josephson L, and Weissleder R (2004). Visualization of antitumor treatment by means of fluorescence molecular tomography with an annexin V–Cy5.5 conjugate. *Proc Natl Acad Sci USA* **101**, 12294–12299.

[9] Choi Y, Weissleder R, and Tung CH (2006). Selective antitumor effect of novel protease-mediated photodynamic agent. *Cancer Res* **15**, 7225–7229.

[10] Choi HK, Yessayan D, Choi HJ, Schellenberger E, Bogdanov A, Josephson L, Weissleder R, and Ntziachristos V (2005). Quantitative analysis of chemotherapeutic effects in tumors using *in vivo* staining and correlative histology. *Cell Oncol* **27**, 183–190.

[11] Callahan R, Bogdanov A, Fischman A, Brady T, and Weissleder R (1998). Preclinical evaluation and phase I clinical trial of a ^{99m}Tc labeled synthetic polymer used in blood pool imaging. *Am J Roentgenol* **171**, 137–143.

[12] Montet X, Figueiredo JL, Alencar H, Ntziachristos V, Mahmood U, and Weissleder R (2007). Tomographic fluorescence imaging of tumor vascular volume in mice. *Radiology* **242**, 751–758.

[13] Nahrendorf M, Sosnovik DE, Waterman P, Swirski FK, Pande AN, Aikawa E, Figueiredo JL, Pittet MJ, and Weissleder R (2007). Dual channel optical tomographic imaging of leukocyte recruitment and protease activity in the healing myocardial infarct. *Circ Res* **100**, 1218–1225.

[14] DeClerck YA, Mercurio AM, Stack MS, Chapman HA, Zutter MM, Muschel RJ, Raz A, Matrisian LM, Sloane BF, Noel A, et al. (2004). Proteases, extracellular matrix, and cancer: a workshop of the path B study section. *Am J Pathol* **164**, 1131–1139.

[15] Marten K, Bremer C, Khazaie K, Sameni M, Sloane B, Tung CH, and Weissleder R (2002). Detection of dysplastic intestinal adenomas using enzyme-sensing molecular beacons in mice. *Gastroenterology* **122**, 406–414.

[16] Ntziachristos V, Turner G, Dunham J, Windsor S, Soubret A, Ripoll J, and Shih HA (2005). Planar fluorescence imaging using normalized data. *J Biomed Opt* **10**, 064007.

[17] Graves EE, Ripoll J, Weissleder R, and Ntziachristos V (2003). A sub-millimeter resolution fluorescence molecular imaging system for small animal imaging. *Med Phys* **30**, 901–911.

[18] Podgorski I and Sloane BF (2003). Cathepsin B and its role(s) in cancer progression. *Biochem Soc Symp* **70**, 263–276.

[19] Castiglioni T, Merino MJ, Elsner B, Lah TT, Sloane BF, and Emmert-Buck MR (1994). Immunohistochemical analysis of cathepsins D, B, and L in human breast cancer. *Hum Pathol* **25**, 857–862.

[20] Pellikainen JM, Ropponen KM, Kataja VV, Kellokoski JK, Eskelinen MJ, and Kosma VM (2004). Expression of matrix metalloproteinase (MMP)-2 and MMP-9 in breast cancer with a special reference to activator protein-2, HER2, and prognosis. *Clin Cancer Res* **22**, 7621–7628.

[21] Scorilas A, Karameris A, Arnogiannaki N, Ardavanis A, Bassilopoulos P, Trangas T, and Talieri M (2001). Overexpression of matrix-metalloproteinase-9 in human breast cancer: a potential favourable indicator in node-negative patient. *Br J Cancer* **84**, 1488–1496.

[22] Vizoso FJ, González LO, Corte MD, Rodríguez JC, Vázquez J, Lamelas ML, Junquera S, Merino AM, and García-Muñiz JL (2007). Study of matrix metalloproteinases and their inhibitors in breast cancer. *Br J Cancer* **96**, 903–911.

[23] Yang M, Baranov E, Jiang P, Sun FX, Li XM, Li L, Hasegawa S, Bouvet M, Al-Tuwaijri M, Chishima T, et al. (2000). Whole-body optical imaging of green fluorescent protein-expressing tumors and metastases. *Proc Natl Acad Sci USA* **97**, 1206–1211.

[24] Piwnica-Worms D, Schuster DP, and Garbow JR (2004). Molecular imaging of host-pathogen interactions in intact small animals. *Cell Microbiol* **6**, 319–331.

[25] Gao XH, Cui YY, Levenson RM, Chung LWK, and Nie SM (2004). *In vivo* cancer targeting and imaging with semiconductor quantum dots. *Nat Biotechnol* **22**, 969–976.

[26] Mayes P, Dicker D, Liu Y, and El-Deiry W (2008). Noninvasive vascular imaging in fluorescent tumors using multispectral unmixing. *Biotechniques* **45**, 459–464.

[27] von Burstin J, Eser S, Seidler B, Meining A, Bajbouj M, Mages J, Lang R, Kind AJ, Schnieke AE, Schmid RM, et al. (2008). Highly sensitive detection of early-stage pancreatic cancer by multimodal near-infrared molecular imaging in living mice. *Int J Cancer* **123**, 2138–2147.

[28] Tsien RY (2005). Building and breeding molecules to spy on cells and tumors. *FEBS Lett* **579**, 927–932.

[29] Achilefu S, Bloch S, Markiewicz MA, Zhong T, Ye Y, Dorshow RB, Chance B, and Liang K (2005). Synergistic effects of light-emitting probes and peptides for targeting and monitoring integrin expression. *Proc Nat Acad Sci USA* **102**, 7976–7981.

[30] Zaheer A, Lenkinski RE, Mahmood A, Jones AG, Cantley LC, and Frangioni JV (2001). *In vivo* near-infrared fluorescence imaging of osteoblastic activity. *Nat Biotechnol* **19**, 1148–1154.

[31] Bhojani MS, Hamstra DA, Chang DC, Coppola JM, Khan AP, Reddy GR, Ross BD, and Rehemtulla A (2006). Imaging of proteolytic activity using a conditional cell surface receptor. *Mol Imaging* **5**, 129–137.

[32] Kovar JL, Volcheck W, Sevick-Muraca E, Simpson MA, and Olive DM (2009). Characterization and performance of a near-infrared 2-deoxyglucose optical imaging agent for mouse cancer models. *Anal Biochem* **384** (2), 254–262.

[33] Ray P, De A, Patel M, and Gambhir SS (2008). Monitoring caspase-3 activation with a multimodality imaging sensor in living subjects. *Clin Cancer Res* **14**, 5801–5809.

[34] Pierce MC, Javier DJ, and Richards-Kortum R (2008). Optical contrast agents and imaging systems for detection and diagnosis of cancer. *Int J Cancer* **123**, 1979–1990.

[35] Zhang S, Metelev V, Tabatadze D, Zamecnik P, and Bogdanov A Jr (2008). Near-infrared fluorescent oligodeoxyribonucleotide reporters for sensing NF-κB DNA interactions *in vitro*. *Oligonucleotides* **18**, 235–243.

[36] Ntziachristos V, Ripoll J, Wang LV, and Weissleder R (2005). Looking and listening to light: the evolution of whole-body photonic imaging. *Nat Biotechnol* **23**, 313–320.